Nucleon momentum distributions in asymmetric nuclear matter

Z. X. Yang,[1,2] X. L. Shang,[1,2,*] G. C. Yong,[1,2] W. Zuo,[1,2] and Y. Gao[3]
[1]*Institute of Modern Physics, Chinese Academy of Sciences, Lanzhou 730000, China*
[2]*School of Nuclear Science and Technology, University of Chinese Academy of Sciences, Beijing 100049, China*
[3]*School of Information Engineering, Hangzhou Dianzi University, Hangzhou 310018, China*

(Received 26 July 2019; published 21 November 2019)

Nucleon momentum distributions at various densities and isospin asymmetries for nuclear matter are investigated systematically within the extended Brueckner-Hartree-Fock approach. The shapes of the normalized momentum distributions varying with k/k_F are practically identical, while the density- and isospin-dependent magnitude of the distribution is directly related to the depletion of the Fermi sea. Based on these properties, a parametrized formula is proposed with the parameters calibrated to the calculated result.

DOI: 10.1103/PhysRevC.100.054325

I. INTRODUCTION

To determine reliably the structure and properties of nuclear matter is one of the central issues in nuclear physics and nuclear astrophysics [1–4]. One of the most important properties of nuclear matter is the neutron and proton momentum distributions which can shed light on the correlations between nucleons [5–8]. In an ideal infinite noninteracting Fermi systems at zero temperature, the momentum distribution is the step function, i.e., $n(k) = \theta(k_F - k)$, and the Fermi sea is fully occupied. Once the interactions are turned on, the correlations induced by the interactions among fermions lead to the occupation of states with momenta $k > k_F$ (the high-momentum distribution) and the depletion of the Fermi sea [9–11]. In addition, the depletion can be directly obtained from the momentum distribution. As for the nuclear matter, due to the hard core and the tensor component of the NN interaction, the depletion of the Fermi sea is quite significant [12,13]. It measures the dynamical NN correlation strength induced by the NN interaction [7], and is believed to be an indicator for testing the validity of physical picture of independent particle motion in the mean-field approach or standard shell model [14,15] in a nuclear many-body system. The knowledge of the momentum distribution in nuclear matter may provide useful information to gain insight into the depletion of the deeply bound state inside finite nuclei and then to understand the structure beyond mean-field theory of finite nuclei. It may also help in the study of the effects of short-range correlations (SRCs) on the observables in heavy-ion reactions [16,17].

Experimentally, the high-momentum distribution and the NN correlations were unambiguously identified in a series of experiments, such as $(e, e'p)$ [18] and $(e, e'NN)$ [19,20]. Especially, the two-nucleon knockout experiment shows that nucleons can form short-range correlated pairs with large relative momenta and small center-of-mass momenta [21]. The number of neutron-proton (np) correlated pairs was found to be about 18 times that of proton-proton (pp) correlated pairs [22–24] which suggests that the tensor correlations due to the strong tensor components of the NN interaction, in addition to SRCs, play also an important role in the high-momentum distributions [25]. In Ref. [8], the authors attempted to distinguish the dominant regions of tensor correlations and SRCs via comparing the momentum distributions of nuclear matter with the deuteron. They found that SRCs tend to dominate the high-momentum distributions above 3 fm^{-1}, while the tensor correlation is of interest in the region of $k \approx 2$–2.8 fm^{-1}. However, both in the theoretical calculations and experiments, the effects of these two correlations on the momentum distribution are hard to distinguished strictly.

In theoretical calculations, the NN correlations in nuclear matter have often been studied in combination with the nucleon momentum distribution. Various theoretical methods have been employed to study these distributions, such as the correlated basis functions [26,27], quantum Monte Carlo method [28], the self-consistent Green's function (SCGF) [8,29–32], the in-medium T-matrix method [33,34], and the extended Brueckner-Hartree-Fock (EBHF) method [5,35–38]. In Ref. [32], the temperature, density, and isospin dependence of the depletion of the Fermi sea is clarified in the framework of SCGF. The momentum distribution at large momentum has been discussed as well which shows an exponential damping tendency. In Ref. [38], the authors have calculated the nucleon momentum distribution and quasiparticle strength in symmetric nuclear matter within the EBHF approach. Parametrized three-section expression of the momentum distribution fit to the microscopic calculation has also been provided. Unfortunately, the parametrization is density independent and merely valid for the symmetric case. In the present paper, we shall extend the parametrized expression of the momentum distribution to asymmetric nuclear matter and simplify the form of the expression of the momentum distribution. Moreover, the density and isospin dependence of the depletion of the Fermi sea is discussed as well within the EBHF approach. In order to

*shangxinle@impcas.ac.cn

obtain a more realistic momentum distribution expression, the calculated momentum distribution within the EBHF approach includes the three-body force (TBF) effects.

This paper is organized as follows. In the next section, we give a brief review of the adopted theoretical approaches including the EBHF theory and spectral function. The formula of the momentum distribution is derived in Sec. III. In Sec. IV, we employ the obtained formula to study the SRC effects on heavy-ion reactions. And finally, a summary is given in Sec. V.

II. THEORETICAL APPROACHES

The present calculations for asymmetric nuclear matter are based on the EBHF approach, for which one can refer to Ref. [39] for details. The extension of the BHF scheme to include microscopic TBF can be found in Refs. [40,41]. After several self-consistent iterations, the effective interaction matrix G in the Brueckner-Bethe-Goldstone (BBG) theory can be obtained. This G matrix, which includes all the ladder diagrams of the NN interaction, embodies the tensor correlations and the SRCs. Using the G matrix, the mass operator $M(k,\omega)$ can be calculated.

A. Mass operator within the extended Brueckner-Hartree-Fock approach

Generally, the nucleon momentum distribution needs the exact knowledge of the mass operator. In practice, it is impossible to calculate the mass operator exactly. In an actual calculation, one can only evaluate some approximations to the mass operator. Within the framework of the BBG theory, the mass operator can be expanded in a perturbation series according to the number of hole lines. To the lowest-order approximation, i.e., the BHF approximation, the mass operator is written as

$$M_1(k,\omega)=\sum_{k'}\theta(k_F-k')\langle kk'|G[\omega+\epsilon(k')]|kk'\rangle_A, \quad (1)$$

where ω is the starting energy and $\epsilon(k)$ represents the single-particle spectrum in the BHF approximation, i.e., $\epsilon(k)=k^2/2m+\mathrm{Re}M_1[k,\epsilon(k)]$. The step function $\theta(k_F-k)$ is the Fermi distribution at zero temperature. The subscript A denotes antisymmetrization of the matrix elements.

The quantity $M_1(k,\omega)$ only has a right-hand cut which is mainly responsible for the depletion under the Fermi surface [11,12]. Therefore, the calculation of the momentum distribution requires at least the first- and second-order approximations of the mass operator. The second order in the hole-line expansion of the mass operator, which might be answerable for the high-momentum distributions above the Fermi surface [11], is given by [39]

$$M_2(k,\omega)=\frac{1}{2}\sum_{k'k_1k_2}\theta(k'-k_F)\theta(k_F-k_1)\theta(k_F-k_2)\times\frac{|\langle kk'|G[\epsilon(k_1)+\epsilon(k_2)]|k_1k_2\rangle_A|^2}{\omega+\epsilon(k')-\epsilon(k_1)-\epsilon(k_2)-i0}, \quad (2)$$

where the step function $\theta(k'-k_F)$ guarantees the integral over k' above the Fermi surface. In the present paper, we calculate the mass operator to the second-order approximation, i.e., $M(k,\omega)\cong M_1(k,\omega)+M_2(k,\omega)$.

B. Spectral function and momentum distribution

The knowledge of $M(k,\omega)$ allows us to write Green's function in the energy-momentum representation

$$\mathcal{G}(k,\omega)=\frac{1}{\omega-\frac{k^2}{2m}-M(k,\omega)}. \quad (3)$$

Generally, the mass operator $M(k,\omega)$ is complex and can be written as

$$M(k,\omega+i\eta)=V(k,\omega)+iW(k,\omega), \quad (4)$$

with the property $[M(k,\omega+i\eta)]^*=M(k,\omega-i\eta)$, where $\eta=+0$ to ensure the integral-path. Using the Lehmann representation for Green's function, the spectral function $S(k,\omega)$, which describes the probability density of removing a particle with momentum k from a target nuclear system and leaving the final system with the excitation energy ω, is thus given by

$$\begin{aligned}S(k,\omega)&=\frac{i}{2\pi}[\mathcal{G}(k,\omega)-\mathcal{G}(k,\omega)^*]\\&=-\frac{1}{\pi}\frac{W(k,\omega)}{[\omega-k^2/2m-V(k,\omega)]^2+W(k,\omega)^2}.\end{aligned} \quad (5)$$

And it should fulfill the sum rule

$$\int_{-\infty}^{\infty}S(k,\omega)d\omega=1. \quad (6)$$

In Ref. [6], the authors show that elaborately dealing with the integral over the energy can satisfy the sum rule quite well by adopting the mass operator up to second order in the framework of the EBHF approach.

Finally, the momentum distribution $n(k)$ is related to the spectral function by

$$n(k)=\int_{-\infty}^{E_F}S(k,\omega)d\omega \quad (7)$$

or

$$n(k)=1-\int_{E_F}^{\infty}S(k,\omega)d\omega, \quad (8)$$

where the Fermi energy E_F follows the on-shell condition $E_F=k_F^2/2m+V(k,E_F)$. The quantities of Eqs. (7) and (8) are identical when the sum rule of the spectral function is fulfilled.

Using the momentum distribution $n(k)$, one can then define the depletion parameter

$$\chi=\left[\sum_{\mathbf{k}}n(k>k_F)\right]\Big/\rho=\left[\frac{1}{\pi^2}\int_{k_F}^{\infty}n(k)k^2dk\right]\Big/\rho, \quad (9)$$

i.e., the proportion of the particle number above the Fermi momentum. This parameter is related to several physical quantities such as the correlation strength or the defect function, and is believed to be an indicator for the convergence of the so-called BBG hole-line expansion.

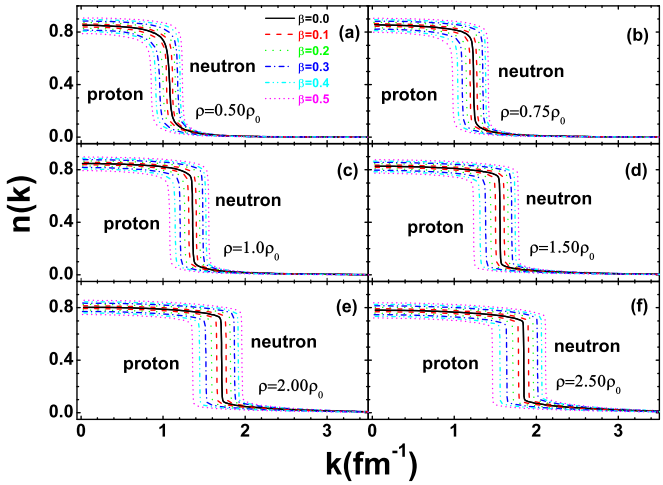

FIG. 1. Neutron and proton momentum distributions in asymmetric nuclear matter at various isospin asymmetries calculated within the EBHF approach for the different densities $0.50\rho_0$, $0.75\rho_0$, $1.0\rho_0$, $1.50\rho_0$, $2.0\rho_0$, and $2.5\rho_0$.

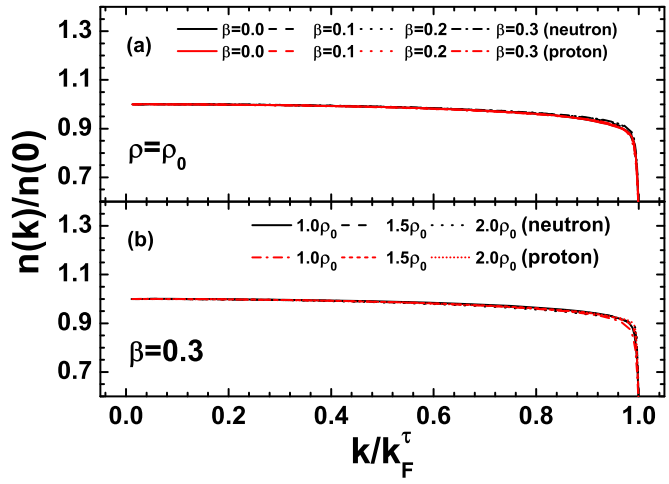

FIG. 2. The normalized momentum distribution $n(k)/n(0)$ vs k/k_F^τ below the Fermi momentum at various isospin asymmetries (upper panel) and at various densities (lower panel).

III. FORMULA FOR MOMENTUM DISTRIBUTION

In this section, we first exhibit the numerical calculation of momentum distributions within the EBHF approach, then roughly analyze the behavior of these distributions, and finally provide a formula for calculating the distribution. The realistic Argonne V18 two-body interaction supplemented with a microscopic TBF [40,41] is taken as the NN interaction. In the present paper, the calculation is under zero temperature.

Generally, the mass operator and the G matrix should be calculated self-consistently to obtain accurately the momentum distribution [11,42,43]. However, a completely self-consistent process is quite difficult to be performed. In our calculations, the G matrix is first self-consistently obtained with the lowest order of the mass operator, i.e., taking $\epsilon(k) = k^2/2m + \mathrm{Re}M_1[k, \epsilon(k)]$ into account in the calculation of the G matrix. Afterward the second-order approximation of the mass operator is calculated. These simplifications might violate the conservation of the number of particles. Fortunately, as in Ref. [6], the spectral functions are found to be almost exactly normalized [the integrations in Eq. (6) are about 0.99] with the help of the extrapolation of the spectral function, which imply that Eqs. (7) and (8) are approximately the same [we adopt Eq. (7) in our calculation]. Moreover, the calculated momentum distribution $n(k)$ fulfills the density sum rule quite well. For symmetric nuclear matter at the saturation density, $3\int_0^\infty n(k)k^2dk/k_F^3 \approx 0.97$.

Now we first systematically report the calculated neutron and proton momentum distributions at various isospin asymmetries $\beta = 0.0$, 0.1, 0.2, 0.3, 0.4, 0.5 with different total densities $0.50\rho_0$, $0.75\rho_0$, $1.0\rho_0$, $1.50\rho_0$, $2.0\rho_0$, $2.5\rho_0$ in Fig. 1. Hereafter, the isospin asymmetry β is defined as $\beta = (\rho_n - \rho_p)/(\rho_n + \rho_p)$ and $\rho_0 = 0.17$ fm^{-3} is the empirical saturation density of nuclear matter. The distributions present a discontinuity at their respective Fermi momenta k_F^τ (hereafter $\tau = n, p$). For positive asymmetries, the neutron Fermi momentum k_F^n is larger than the proton Fermi momentum k_F^p, therefore the proton and neutron momentum distributions are located at the left and right sides of the symmetric case, respectively. One should note that the neutron momentum distribution differs only slightly from proton momentum distribution in the symmetric case due to the charge-dependent interaction Argonne V18. The discrepancy is too tiny to be recognized in the figures.

Interestingly, if focusing on the shapes of the momentum distributions in Fig. 1, one would notice that these distributions are quite similar except for the magnitudes. Inspired by this quality, we show the normalized momentum distributions $n(k)/n(0)$ as a function of the ratio k/k_F^τ below the Fermi momentum at various isospin asymmetries and densities in Fig. 2. Where k_F^τ is the respective Fermi momentum corresponding to the different isospin asymmetry β and density ρ. The shapes of the normalized distributions are practically identical except for slightly small discrepancies near the Fermi momentum. In Fig. 3, the same normalized momentum distributions as in Fig. 2 but above the Fermi moment exhibit the coincidence of the shapes as well. In other words, the normalized momentum distributions as a function of the ratio k/k_F^τ below (above) the Fermi momentum at various densities and isospin asymmetries can be described by the same expression with tolerable errors. In the domain $0 < k/k_F^\tau < 1$, the normalized momentum distribution varying with k/k_F^τ below the Fermi momentum can be described by the following parametrization:

$$\frac{n_<^\tau(k)}{n(0)} = 1.00329 - 0.02876x - 0.09053x^7, \qquad (10)$$

where $n_<^\tau(k)$ corresponds to $n(k < k_F^\tau)$ and x represents the ratio k/k_F^τ. A comparison between the calculated $n_<^\tau(k)/n(0)$ and the parametrization is shown in the upper panel of Fig. 4. The polynomial fit is in good agreement with the calculation within the EBHF approach.

For the high-momentum distributions, i.e., $k > k_F^\tau$, Ref. [44] reports that the momentum distributions appear to decrease as k^{-4}, following Tan's relation [45,46]. However,

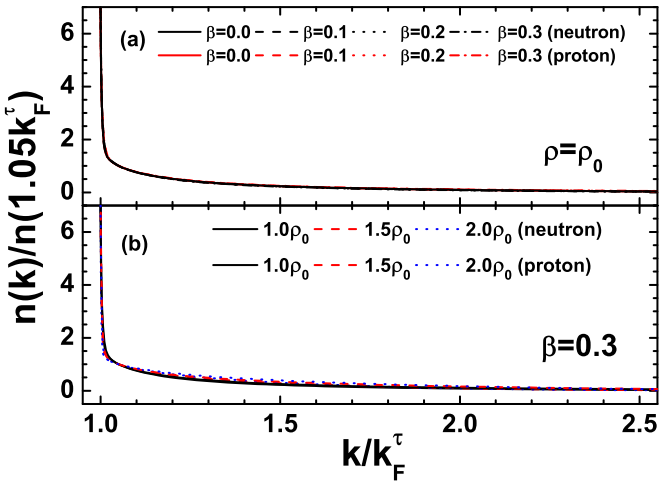

FIG. 3. The normalized momentum distribution $n(k)/n(1.05k_F^\tau)$ vs k/k_F^τ above the Fermi momentum at various isospin asymmetries (upper panel) and various densities (lower panel).

Tan's relation is simply valid for a dilute system with contact interaction whereas the *NN* interaction is much more complicated. And the microscopic calculations including the EBHF approach [38] and the SCGF method [8,32] indicate a nearly linear relation between $\ln n(k)$ and k at large momentum, i.e., $n(k) \propto \exp(-ck)$ (c is a positive constant). In addition, if one adopts the form of k^{-4} to describe the high-momentum distributions, a cutoff k_Λ is always supplemented owing to the slow convergence of the number density. When k_Λ is employed, the neglected number density is

$$\int_{k_\Lambda}^{\infty} n(k)k^2dk \propto \frac{1}{k_\Lambda} \ . \tag{11}$$

In calculations, the maximum value of k_Λ is usually about 5 fm^{-1}, which implies 3–5% is missing of the number density. Most importantly, our calculations within the EBHF approach

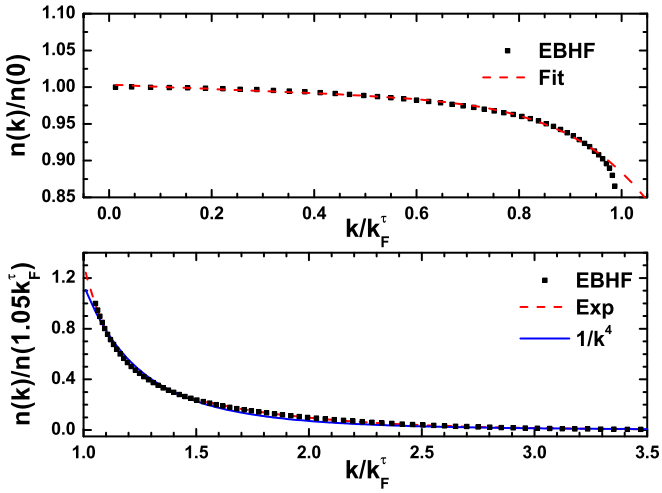

FIG. 4. The normalized distributions as a function of k/k_F^τ and the fittings. The upper and the lower panels correspond to the momentum below and above the momentum, respectively.

reveal the same behavior of the high-momentum distributions as Ref. [38]. For the above reasons, we employ the exponential form replenished by a Gauss function to describe the high-momentum behavior. The normalized momentum distribution above the Fermi momentum can be expressed as

$$\frac{n_>^\tau(k)}{n\left(1.05k_F^\tau\right)} = 3.548e^{-1.799x} + 52.2e^{-4.2766x^2}, \tag{12}$$

with $n_>^\tau(k) \equiv n(k > k_F^\tau)$ and $x \equiv k/k_F^\tau$. We display the expression of k^{-4} ($1/k^4$), the parametrization (12) (Exp) and the calculation within EBHF approach in the lower panel of Fig. 4. Obviously, the exponential fit is more approaching to the calculation than the k^{-4} fit. But we should stress that owing to the approximations adopted in the calculations and fittings, the possibility of Tan's relation in nucleon momentum distribution could not be ruled out.

To obtain the momentum distributions, the magnitudes of $n(k)$ below and above the Fermi momentum remain to be identified once the shapes are provided. Actually, the magnitudes connect with the depletion parameter χ via the relations

$$\begin{aligned} 1-\chi &= \frac{\frac{1}{\pi^2}\int_0^{k_F^\tau} n_<^\tau(k)k^2dk}{\rho_\tau} \\ &= 3\int_0^1 n_<^\tau(k)x^2dx = 0.9546n(0), \end{aligned} \tag{13}$$

$$\begin{aligned} \chi &= \frac{\frac{1}{\pi^2}\int_{k_F^\tau}^{\infty} n_>^\tau(k)k^2dk}{\rho_\tau} \\ &= 3\int_1^{\infty} n_>^\tau(k)x^2dx = 2.9537n\left(1.05k_F^\tau\right). \end{aligned} \tag{14}$$

Consequently, the magnitudes of the $n(k)$ below and above the Fermi momentum are directly related to the depletion parameter, i.e.,

$$n(0) = \frac{1-\chi}{0.9546}, \quad n\left(1.05k_F^\tau\right) = \frac{\chi}{2.9537}. \tag{15}$$

The depletion parameter χ calculated within the EBHF approach with various isospin asymmetries $\beta = 0.0$, 0.1, 0.2, 0.3, 0.4, and 0.5 at two typical densities ρ_0 and $2.0\rho_0$ are exhibited in Fig. 5. Obviously, the proton (neutron) depletion of the Fermi sea increases (decreases) almost linearly with varying isospin asymmetry. Due to Eq. (15), $n(0)$ demonstrates the analogous behavior reported in Refs. [5,47]. The experiments show that the np correlation is much stronger than nn or pp correlations [23,24]. One should notice that the probability of a proton (neutron) encountering a neutron (proton) increases (decreases) linearly as a function of isospin asymmetry. If supposing equal correlation in each correlated np pair and neglecting the nn and pp correlations, the linear isospin dependence of χ comes very naturally. In Fig. 6 we illustrate the density dependence of the depletion parameter. The different types of dots correspond to the calculated χ within the EBHF approach. According to the shapes of χ varying with ρ, we propose an expression with the parameters

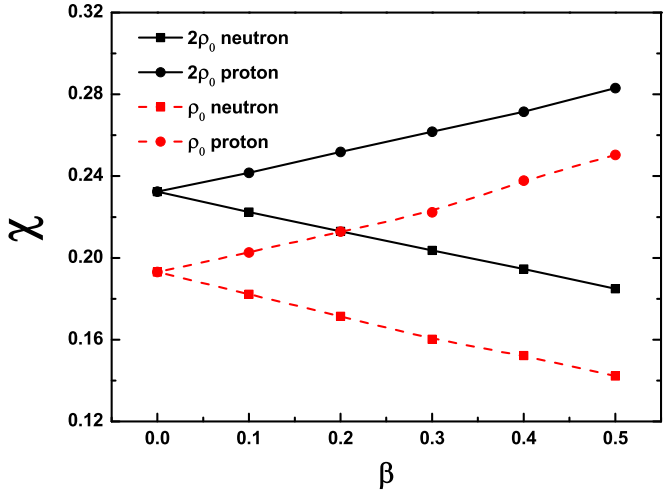

FIG. 5. The depletion parameter χ calculated within the EBHF approach varying with isospin asymmetry β for two densities ρ_0 and $2.0\rho_0$.

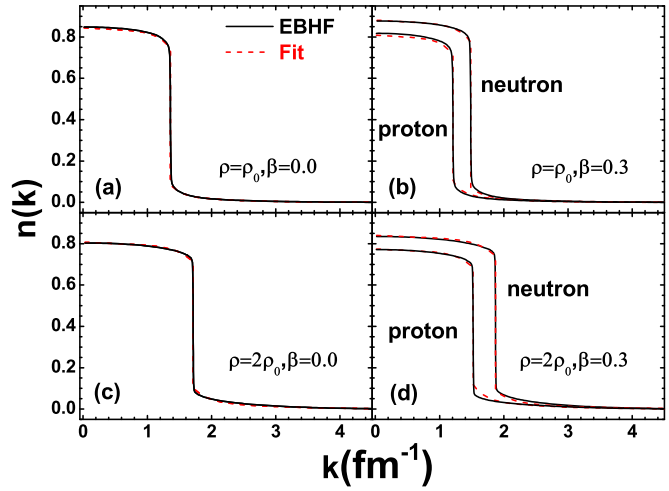

FIG. 7. Neutron and proton momentum distributions from the formula (17) and the calculation within the EBHF approach at two isospin asymmetries and densities.

calibrated to the calculated χ. The expression reads

$$\chi(\rho,\beta) = 0.1669\left[1+\lambda\left(0.1407\frac{\rho}{\rho_0}-0.7296\right)\beta\right] \times\left[1+2.448e^{-4.1854\frac{\rho}{\rho_0}}+0.1382\left(\frac{\rho}{\rho_0}\right)^{1.5}\right]. \tag{16}$$

Where $\lambda = 1$ (-1) corresponds to neutron (proton). The isospin and density dependence of χ are mainly included in the first and second square brackets on the right-hand side of Eq. (16), respectively. One would find that there is a slight discrepancy between the slopes of curves in Fig. 5 indicating a weak density dependence of $\partial\chi/\partial\beta$. We actually account for this dependence in the first square bracket of Eq. (16). In fact, a simple analysis of the calculated data on the density dependence of the slope reveals a roughly linear dependence. In Ref. [8], the authors have also mentioned a similar behavior of momentum distribution in asymmetric nuclear matter at finite temperature. The expression (16) for various densities and isospin asymmetries is shown by lines in Fig. 6. Below the saturation density, the depletion of the Fermi sea becomes stronger with decreasing density which might mainly result from the increasing effect of the tensor correlation. While above the saturation density, the hard-core effect and the depletion get larger and larger with increasing density [7].

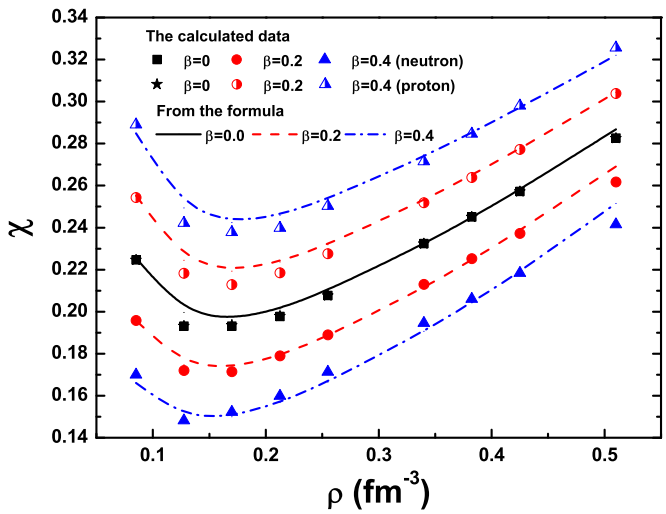

FIG. 6. The depletion parameter χ vs densities. The symbols correspond to the calculations within the EBHF approach. The lines are obtained from Eq. (16). The upper and lower lines are related to protons and neutrons, respectively.

Finally, the formula of the momentum distribution can be summarized as

$$n(k) = \begin{cases} \frac{1-\chi}{0.9546}\left[1.00329-0.02876\frac{k}{k_F^\tau}-0.09053\left(\frac{k}{k_F^\tau}\right)^7\right] \\ \text{if } k \leqslant k_F^\tau, \\ \frac{\chi}{2.9537}\left[3.548e^{-1.799\frac{k}{k_F^\tau}}+52.2e^{-4.2766\left(\frac{k}{k_F^\tau}\right)^2}\right] \\ \text{if } k \geqslant k_F^\tau, \end{cases} \tag{17}$$

with the expression of the depletion parameter of Eq. (16). A comparison between the momentum distributions from formula (17) and from the EBHF approach is given in Fig. 7. It can be clearly seen that the formula is quite accurate except for a slight difference near the Fermi momentum. This formula can be applied to calculate the momentum distribution in finite nuclei assisted by the local density approximation. As is well known, at low densities the nuclear matter system can minimize its energy by forming light clusters such as deuterons, or particularly strongly bound α particles [48]. In theoretical calculations such as the EBHF approach, the in-medium T-matrix method, and the SCGF method, the effective interaction including all the ladder-diagram contribution always encounters a singularity leading to unstable results at low densities [49,50]. Therefore, we emphasize that the achieved formula (17) of the momentum distribution might be solely reliable for the density of $0.1\rho_0 < \rho < 3.0\rho_0$ and

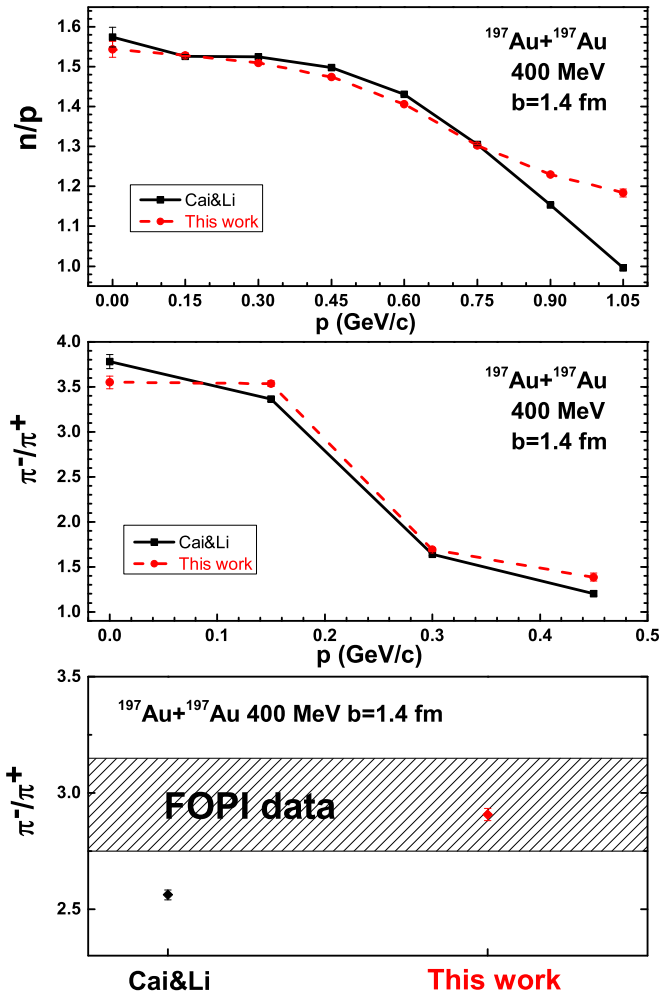

FIG. 8. Upper panel: Free neutron to proton ratio as a function of momentum in the central Au + Au reaction at 400 MeV/nucleon. Middle panel: Same as upper panel, but for π^-/π^+ ratio. Lower panel: Comparison of calculated total π^-/π^+ yields ratios and FOPI data [53].

the isospin asymmetry of $\beta \in (-0.5, 0.5)$ for uniform nuclear matter. Otherwise, one should be careful of the depletion parameter.

IV. APPLICATION TO THE TRANSPORT MODEL

As an example of application, the obtained density- and asymmetry-dependent nucleon momentum distribution of Eq. (17) and the fraction of high-momentum nucleons from Eq. (16) were both involved in the isospin-dependent Boltzmann-Uehling-Uhlenbeck (IBUU) transport model [51]. The free neutron to proton ratio and the π^-/π^+ ratio as a function of momentum in the central Au + Au reaction at 400 MeV/nucleon are demonstrated in the upper and middle windows of Fig. 8. As comparisons, the nucleon momentum distribution from Cai *et al.* is also used [17,52]. The lower window shows the integrations of the π^-/π^+ ratio and comparison with the FOPI data [53]. From Fig. 8, with the formula (17) and the work of Cai *et al.*, it is seen that both the momentum distribution of the free n/p ratio and the π^-/π^+ ratio are quite similar, except for energetic n/p ratio. While the difference of the total π^-/π^+ yields ratios is evidently shown in the lower window of Fig. 8. The value of the π^-/π^+ yields ratio with formula (17) is higher than that with the formula of Cai *et al.*. The reason is that the fraction of high-momentum nucleons with formula (17) is smaller than that with the formula of Cai *et al.* [52] and a larger number for the neutron-proton correlation causes a lower value of the π^-/π^+ ratio in heavy-ion collisions.

V. SUMMARY AND OUTLOOK

In summary, we have systematically calculated the nucleon momentum distributions and the depletions of the Fermi sea at various densities and isospin asymmetries for nuclear matter within the EBHF approach. The identity of these shapes of the normalized momentum distributions below (above) the Fermi momentum varying with k/k_F is detected, indicating a uniform expression of the momentum distribution for different densities and isospin asymmetries. Whereas the magnitude of the momentum distribution is directly related to the depletion of the Fermi sea, which first decreases and then increases with densities resulting from the tensor and hard core effects of the NN interaction [7]. Using these properties, the parametrized formula of momentum distribution is proposed with the expression of the depletion. Moreover, a heavy-ion reaction example adopting the obtained formula is given to test its reliability.

In the present paper, the mass operator is just calculated up to the second order, the missing higher order perhaps enhances the depletion of the Fermi sea and eventually influences the momentum distribution. Especially, the missing higher order might also reduce the particle strength around the Fermi surface [54]. Thus, the parametrized formula cannot be considered as definite. In addition, the calculation is based on realistic Argonne V18 only. With different interactions, the depletions of the Fermi sea and the momentum distributions would differ from each other [7,8,32]. Furthermore, the normal state of symmetric nuclear matter becomes unstable owing to the pairing tendency of np [49,50,54,55] and one should account for the effect of the pairing on the momentum distribution. An improvement of the calculations including these effects is under way.

ACKNOWLEDGMENTS

The work is supported by National Natural Science Foundation of China (Grants No. 11435014, No. 11505241, No. 11875013, No. 11775276, No. 11775275, No. 11975282, and No. 11705240), and the Youth Innovation Promotion Association of Chinese Academy of Sciences.

[1] B. A. Li, L. W. Chen, and C. M. Ko, Phys. Rep. **464**, 113 (2008).
[2] I. Bombaci and U. Lombardo, Phys. Rev. C **44**, 1892 (1991).
[3] A. Ramos, A. Polls, and W. H. Dickhoff, Nucl. Phys. A **503**, 1 (1989).

[4] M. Baldo and H. R. Moshfegh, Phys. Rev. C **86**, 024306 (2012).
[5] P. Yin, J. Y. Li, P. Wang, and W. Zuo, Phys. Rev. C **87**, 014314 (2013).
[6] P. Wang and W. Zuo, Phys. Rev. C **89**, 054319 (2014).
[7] Z. H. Li and H.-J. Schulze, Phys. Rev. C **94**, 024322 (2016).
[8] A. Rios, A. Polls, and W. H. Dickhoff, Phys. Rev. C **89**, 044303 (2014).
[9] A. B. Migdal, Zh. Eksp. Teor. Fiz. (USSR) **32**, 339 (1957) [Sov. Phys. JETP **5**, 333 (1957)].
[10] J. M. Luttinger, Phys. Rev. **119**, 1153 (1960).
[11] C. Mahaux and R. Sartor, Phys. Rep. **211**, 53 (1992).
[12] J. P. Jeukenne, A. Lejeune, and C. Mahaux, Phys. Rep. **25**, 83 (1976).
[13] B. E. Vonderfecht, W. H. Dickhoff, A. Polls, and A. Ramos, Phys. Rev. C **44**, R1265 (1991); Nucl. Phys. A **555**, 1 (1993).
[14] V. R. Pandharipande, I. Sick, and P. K. A. deWitt Huberts, Rev. Mod. Phys. **69**, 981 (1997).
[15] J. M. Cavedon, B. Frois, D. Goutte *et al.*, Phys. Rev. Lett. **49**, 978 (1982).
[16] G. C. Yong and B. A. Li, Phys. Rev. C **96**, 064614 (2017).
[17] Z. X. Yang, X. H. Fan, G. C. Yong, and W. Zuo, Phys. Rev. C **98**, 014623 (2018).
[18] D. Rohe *et al.*, Phys. Rev. Lett. **93**, 182501 (2004).
[19] C. J. G. Onderwater *et al.*, Phys. Rev. Lett. **81**, 2213 (1998).
[20] R. Starink *et al.*, Phys. Lett. B **474**, 33 (2000).
[21] R. Shneor *et al.*, Phys. Rev. Lett. **99**, 072501 (2007).
[22] E. Piasetzky, M. Sargsian, L. Frankfurt, M. Strikman, and J. W. Watson, Phys. Rev. Lett. **97**, 162504 (2006).
[23] R. Subedi *et al.*, Science **320**, 1476 (2008).
[24] O. Hen *et al.* (CLAS Collaboration), Science **346**, 614 (2014).
[25] R. Schiavilla, R. B. Wiringa, S. C. Pieper, and J. Carlson, Phys. Rev. Lett. **98**, 132501 (2007).
[26] S. Fantoni and V. Pandharipande, Nucl. Phys. A **427**, 473 (1984).
[27] O. Benhar, A. Fabrocini, and S. Fantoni, Nucl. Phys. A **505**, 267 (1989); Phys. Rev. C **41**, R24 (1990).
[28] A. Gezerlis and J. Carlson, Phys. Rev. C **81**, 025803 (2010).
[29] Y. Dewulf, D. Van Neck, and M. Waroquier, Phys. Rev. C **65**, 054316 (2002); Y. Dewulf, W. H. Dickhoff, D. Van Neck, E. R. Stoddard, and M. Waroquier, Phys. Rev. Lett. **90**, 152501 (2003).
[30] T. Frick, H. Müther, A. Rios, A. Polls, and A. Ramos, Phys. Rev. C **71**, 014313 (2005).
[31] A. Rios, A. Polls, and I. Vidana, Phys. Rev. C **79**, 025802 (2009).
[32] A. Rios, A. Polls, and W. H. Dickhoff, Phys. Rev. C **79**, 064308 (2009).
[33] P. Bozek, Phys. Rev. C **59**, 2619 (1999); **65**, 054306 (2002).
[34] V. Soma and P. Bozek, Phys. Rev. C **78**, 054003 (2008).
[35] R. Sartor and C. Mahaux, Phys. Rev. C **21**, 1546 (1980); P. Grangé, J. Cugnon, and A. Lejeune, Nucl. Phys. A **473**, 365 (1987); M. Jaminon and C. Mahaux, Phys. Rev. C **41**, 697 (1990); M. Baldo, I. Bombaci, G. Giansiracusa, and U. Lombardo, Nucl. Phys. A **530**, 135 (1991); C. Mahaux and R. Sartor, *ibid.* **553**, 515 (1993).
[36] Kh. S. A. Hassaneen and H. Müther, Phys. Rev. C **70**, 054308 (2004).
[37] P. Wang, S.-X. Gan, P. Yin, and W. Zuo, Phys. Rev. C **87**, 014328 (2013).
[38] M. Baldo, I. Bombaci, G. Giansiracusa, U. Lombardo, C. Mahaux, and R. Sartor, Phys. Rev. C **41**, 1748 (1990); Nucl. Phys. A **545**, 741 (1992).
[39] W. Zuo, I. Bombaci, and U. Lombardo, Phys. Rev. C **60**, 024605 (1999).
[40] P. Grangé, A. Lejeune, M. Martzolff, and J.-F. Mathiot, Phys. Rev. C **40**, 1040 (1989).
[41] W. Zuo, A. Lejeune, U. Lombardo, and J.-F. Mathiot, Nucl. Phys. A **706**, 418 (2002); Eur. Phys. J. A **14**, 469 (2002).
[42] R. Sartor, Nucl. Phys. A **289**, 329 (1977).
[43] M. Baldo, I. Bombaci, L. S. Ferreira, G. Giansiracusa, and U. Lombardo, Phys. Lett. B **209**, 135 (1988).
[44] O. Hen, L. B. Weinstein, E. Piasetzky, G. A. Miller, M. M. Sargsian, and Y. Sagi, Phys. Rev. C **92**, 045205 (2015).
[45] S. Tan, Ann. Phys. **323**, 2952 (2008); **323**, 2971 (2008); **323**, 2987 (2008).
[46] J. T. Stewart, J. P. Gaebler, T. E. Drake, and D. S. Jin, Phys. Rev. Lett. **104**, 235301 (2010).
[47] H. Müther, G. Knehr, and A. Polls, Phys. Rev. C **52**, 2955 (1995).
[48] S. Typel, G. Ropke, T. Klahn, D. Blaschke, and H. H. Wolter, Phys. Rev. C **81**, 015803 (2010).
[49] V. J. Emery, Nucl. Phys. A **12**, 69 (1959); H. F. Arellano and J. P. Delaroche, Eur. Phys. J. A **51**, 7 (2015).
[50] W. H. Dickhoff, Phys. Lett. B **210**, 15 (1988); B. E. Vonderfecht, C. C. Gearhart, W. H. Dickhoff, A. Polls, and A. Ramos, *ibid.* **253**, 1 (1991).
[51] G. C. Yong, Phys. Rev. C **96**, 044605 (2017).
[52] B. J. Cai, B. A. Li, and L. W. Chen, Phys. Rev. C **94**, 061302(R) (2016).
[53] W. Reisdorf *et al.* (FOPI Collaboration), Nucl. Phys. A **848**, 366 (2010).
[54] X. H. Fan, X. L. Shang, J. M. Dong, and W. Zuo, Phys. Rev. C **99**, 065804 (2019).
[55] X. L. Shang and W. Zuo, Phys. Rev. C **88**, 025806 (2013); X. L. Shang, P. Wang, P. Yin, and W. Zuo, J. Phys. G: Nucl. Part. Phys. **42**, 055105 (2015).